applied optics

Advanced iterative algorithm for phase calibration of spatial light modulators integrated in optical instrumentation in a vibration environment

Manuel Silva-López,[1,*] Néstor Uribe-Patarroyo,[2] and Alberto Álvarez-Herrero[1]

[1]Departamento de Óptica Espacial, Instituto Nacional de Técnica Aeroespacial INTA, Torrejón de Ardóz 28850 Madrid, Spain
[2]Wellman Center for Photomedicine, Harvard Medical School and Massachusetts General Hospital, 40 Blossom Street, Boston, Massachusetts 02114, USA
*Corresponding author: silvalm@inta.es

Received 11 March 2020; revised 25 June 2020; accepted 29 June 2020; posted 30 June 2020 (Doc. ID 391723); published 30 July 2020

We present a method to obtain the phase modulation characteristic curve of a spatial light modulator (SLM) under severe vibration conditions. The procedure is based on the well-known advanced iterative algorithm (AIA), which allows wavefront extraction from unknown phase-shifted interferograms. Generally, AIA is used to determine the wavefront and the determined phase shifts are of little interest. In contrast, in our method, the main goal of using AIA is to determine the unknown phase shifts induced by an SLM during the calibration procedure. Using a segmented approach to calibration, AIA enables successful calibration even in the presence of additional random phase shifts due to environmental changes. This method has the potential to calibrate SLMs integrated in complex optical instruments with little to no modifications to the optical setup, no matter the environmental conditions. We demonstrate our technique by calibrating an SLM under vacuum conditions (10^{-5} mbar) in a common-path configuration compatible with usage of an SLM as a wavefront modulator at the pupil plane of an instrument. Our technique compensates for the vibrations produced by the vacuum pumps and reduces an order of magnitude the root-mean-squared error of the calibration curve evaluated with vibration errors. Our technique enhances the potential use of SLMs in complex optical systems, including aerospace optical instrumentation. © 2020 Optical Society of America

https://doi.org/10.1364/AO.391723

Provided under the terms of the OSA Open Access Publishing Agreement

1. INTRODUCTION

Liquid-crystal-on-silicon spatial light modulators (LCOS-SLMs) combine the potential of reflection-type SLMs with the compactness and robustness of a single chip. They are used for optical metrology, laser processing, and beam shaping [1–3]. Moreover, in space applications, there is a strong demand for compact electro-optical devices [4,5]. SLMs may save complexity and weight, and reduce the risk associated with the wear of moving parts, such as focusing mechanisms [6]. Alternatively, in communications systems, SLMs have allowed the development of non-mechanical laser beam steering technology, which provides advantages for establishing satellite-to-ground data links [7,8]. Finally, control of the light's orbital angular momentum can be achieved by means of SLMs for quantum communications and information processing [9].

SLMs possess a structure where a liquid crystal layer, serving as the light modulating element, is arranged on an electrically addressing part formed by complementary metal–oxide-semiconductor (CMOS) technology. This is an active matrix circuit that applies voltage to the pixel electrodes. The amount of phase modulation varies according to the applied voltage level. Accordingly, the phase modulation characteristic curve is a key SLM figure of merit that requires to be accurately determined. SLMs are generally driven with a video signal, and the gray level of the incoming video signal is typically converted to voltage using a lookup table. This is necessary to linearize the phase response or to adapt the phase shift range, which depends on working conditions, such as the required modulation range or the operating wavelength. It is known that the calibration curve depends on temperature and other environmental parameters [10,11]. Critically, the introduced phase shift also depends on the incident angle, and thus, for optical systems that use SLMs at non-normal angles of incidence, calibration at the specific opto-mechanical configuration may be needed for optimal performance [12].

SLMs are attractive devices for space instrumentation because they can be used to forgo mechanisms (e.g., focusing mechanisms) while reducing mass, volume, and power requirements. Although LCOS-SLMs are typically too slow for adaptive

optics, SLMs can also be used to implement active optic systems in order to increase the instrument optical performance. Nevertheless, a calibration method for these devices after integration in the instrument are required to be able to perform on-ground end-to-end calibrations and calibrations during the flight. SLMs need to be calibrated within a specific optical configuration of the instrument (incidence angle, collimation degree, pupil position, etc.) because the calibration has a strong dependence on these optical parameters. A calibration method for SLMs used in space instrumentation has to be robust to random phase shifts introduced by the environment: vibrations due to external elements (e.g., vacuum pumps, satellite jitter noise). Note that these issues are not exclusive to space instrumentation, but they are also present in many other on-ground optical systems.

A number of calibration procedures for SLMs have been described in the literature. Among them, procedures based on diffraction, cross polarizers, and interferometry have been developed [11,13–15]. They all have their own merits and difficulties. Phase shifting interferometry (PSI), in particular, though highly accurate, requires a specific configuration that may not be accessible in finished optical instrumentation. PSI is also susceptible to vibrations [16]: in production environments, interferogram vibrations can cause fringe print-through on the data, and prevent reliable phase recovery. As a consequence, and to cope with phase shift errors caused by imperfect phase shifting mechanisms, vibrations or other ambient induced variations, a number of self-calibrating algorithms have been developed. For instance, model-based PSI has been developed to account for specific rigid body motions of the surface that make up the interferometric cavity [17]. For extreme vibrations, instantaneous measurement methods, such as the carrier fringe method, are more appropriate [18].

Some PSI methods have been developed to allow wavefront reconstruction in the presence of unknown phase shifts, such as the advanced iterative algorithm (AIA) [19]. We have shown in the past that AIA can take advantage of the presence of uncontrolled mechanical displacements to recover the wavefront error [20]. This technique has been used to evaluate the wavefront error of a liquid-crystal-based polarization modulator in a space mission environment [21]. During the AIA iterative process, among other parameters, the actual phase shifts among interferograms are determined, but normally discarded, as they provide no useful information.

In the present work, we show a novel usage of AIA that makes use of this often discarded information. Rather than focusing on wavefront error determination, we use a flexible optical configuration to relate the SLM calibration curve directly to the unknown phase shifts among interferograms determined during the AIA procedure. Our approach permits the calibration of SLMs already integrated into complex optical instruments, where other methods cannot be applied. Our method can be used even in harsh environmental conditions, enabling calibration of SLMs during end-to-end testing of complete optical systems. We experimentally simulated the use of our technique to calibrate an SLM in vacuum conditions. In this environment, the SLM may suffer from liquid crystal leakage, outgassing, or other varying phase response issues. As a consequence, a close monitoring of the SLM performance or degradation is mandatory. By dividing the SLM into zones, coupled with a common-path arrangement recently reported [15], we were able to determine the introduced phase shifts as a function of gray-level accurately, even in the presence of strong vibrations. Compared to the technique proposed by Martínez *et al.*, our method clearly improves the accuracy of the phase characteristic measurement. The used SLM successfully completed a vacuum test campaign, demonstrating that SLM technology can be vacuum compatible. We believe this demonstration opens the possibility not only for on-ground end-to-end testing of complete instruments with integrated SLMs where other methods are not applicable, but also to future in-flight calibration procedures.

2. MATERIALS AND METHODS

A. Phase Modulation Calibration Method

The core of our technique is the use of AIA to determine the phase modulation characteristic curve using the SLM as a phase-shifter device introducing unknown phase shifts. This approach works in any interferometric setup, although in Section 2.B, we focus on a common-path configuration. Generally speaking, there is a reference beam E_r (either by a discrete reference mirror or generated in a common-path configuration), and we separate the SLM display into two segments: a modulation segment E_m and an environmental reference segment E_e. During the calibration procedure, the voltage—gray level—of the environmental reference segment is kept at a constant level. Meanwhile, modulated segment sweeps the voltage range (typically gray levels from 0 to $2^8 - 1$). Thus a total of 2×256 interferograms are captured, 256 for each segment. The optical system is arranged in order to have interference fringes resolved by a camera between beams E_r and E_m and between E_r and E_e, which are given for interferogram i as

$$I_{m_i} = |E_r + E_m|^2 = b_m + \mu_m \cos(\phi + \delta_{\mathrm{cal}_i} + \delta_{e_i}), \quad (1)$$

$$I_{e_i} = |E_r + E_e|^2 = b_e + \mu_e \cos(\phi + \delta_{e_i}). \quad (2)$$

We focus in the following on the phase differences terms δ_{cal_i}, which is the gray-level dependent phase shift introduced by the SLM, and δ_{e_i}, which is the stochastically varying phase shift due to the environment. ϕ is a frame-independent offset that is given by the specific optical configuration. We assume ϕ, to an excellent approximation, to be equal for both sides of the SLM. We also define the total phase shift for the modulating segment as $\delta_{\mathrm{m}_i} = \delta_{\mathrm{cal}_i} + \delta_{e_i}$.

As illustrated in Fig. 1, the calibration method is divided into three steps. First we apply the AIA to the set of interferograms I_{e_i} of the environmental reference segment. After the iterative procedure, AIA converges to a solution for which we keep the set of calculated phase shifts (δ_{e_i}), where $i = 1 \ldots 256$. In ideally stable conditions these interferograms are identical (no relative phase shifts), but due to environmental changes within the optical path, the fringes move and the values are variable.

In the second step we apply the AIA to the interferogram area corresponding to the modulated segment, set I_{m_i}. Here the AIA employs δ_{e_i} as a seed, and its output is a list of phase shifts labeled δ_{m_i}. In ideal stable conditions, we could obtain the

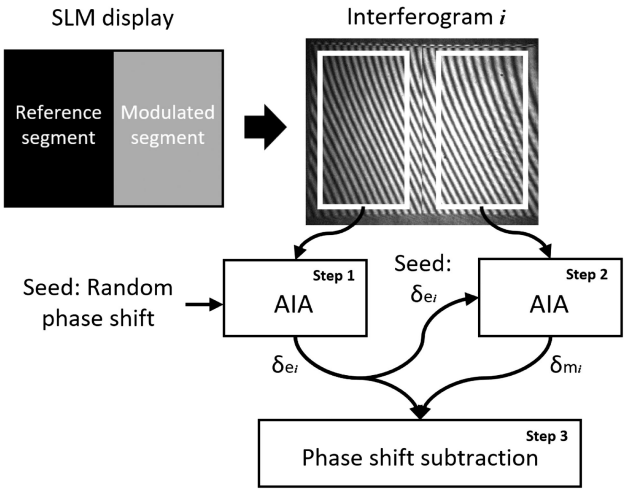


Fig. 1. Phase modulation calibration method. The interferograms are divided into two sections. A fringe discontinuity can be seen between the modulated and the reference segment. This latter segment acts as a noise monitor detector by means of the AIA.

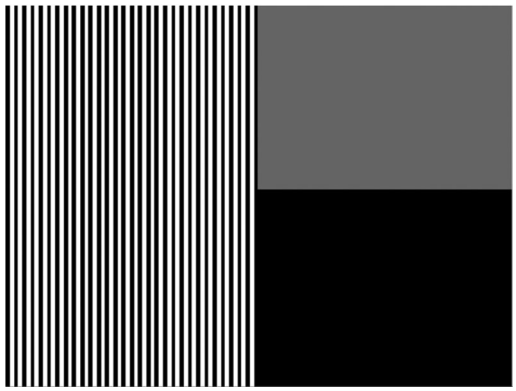


Fig. 2. Pattern sent to the SLM to employ our methodology. Left half displays a binary grating. The bottom section of the right half shows the reference segment (constant value) and the upper section the modulated segment (with variable gray level). The diffracted beam from the left half interferes with the reflection from both segments, yielding the interferograms.

calibration curve directly from this set of phase shifts; however, perturbations to the optical path make this unfeasible, as we obtain $\delta_{\mathrm{cal}_i} + \delta_{e_i}$ [see Eq. (1)].

The third step is to subtract the phase shifts obtained in steps one and two. At this point, we have performed the phase shift compensation, and we obtain the phase modulation characteristic curve of the SLM without the noise contribution δ_{cal_i}. By using one section as a noise monitor detector we are able to subtract the vibration influence very efficiently. Note that we are assuming that the phase shift induced by the environment is identical in both segments at a given time.

Additionally, although a full device characterization requires evaluation of the phase-response inhomogeneity [22,23], we do not consider this effect here. We discuss later how this can be easily incorporated into our procedure. We emphasize that both segments are extracted from the same interferogram (image); thus, the acquisition of the environmental reference and the modulated segments is performed simultaneously. It is the post-processing that is performed in sequence. Finally, and in order to calibrate the whole SLM effective area, the process should be repeated with the segments exchanged.

It must be added that the total calibration time depends on the liquid crystal response time which, for our particular device is on the order of 10 ms [5]. For a 256-level modulator, this yields a few seconds for a complete calibration. This time is effectively doubled since we perform the calibration of one half of the effective area at a time.

Although usage of AIA for this purpose is compatible with many configurations, we focus here on one that uses common-path interferometry to enable the calibration of an SLM already integrated into a complex optical system with minimal to no modifications to the optical setup. Our configuration is based on that reported by Martínez *et al.* [15] and shown in Fig. 2. This allows us to forgo the requirement for a Michelson-type interferometer to perform the calibration procedure, and use the SLM to generate common-path interferometry. However, due to the requirement to generate a reference beam with the SLM itself, the modulating area of the SLM in divided into *three* different segments (see Fig. 2). In this configuration, one half of the SLM surface is used to display a binary grating, which generates the reference beam in near common path made to interfere with the reflection of the second half of the SLM. This second half is further divided into two halves, one displaying a time-variable gray level—the modulating segment—and the other a fixed gray level—the environmental reference segment. A set of interferograms is captured as the gray level is changed from zero to 255. As a consequence, no reference mirror or second interferometer arm is required. The interferometer robustness arises from the near-common-path arrangement.

It is possible to envision strategies to determine the homogeneity of the phase calibration characteristic curve using our approach. Instead of using a modulating segment of a size one-fourth of the total SLM area, it can be reduced to a small area, say 50×50 px, and perform the calibration procedure. This small modulating area can then be swept across the SLM active area to determine a spatially resolved calibration curve.

B. Experimental Setup

The experimental setup is shown in Fig. 3. The modulator comes in a compact head of $74 \times 39 \times 110\ \mathrm{mm}^3$ external dimensions. The active area is formed of a glass substrate, a transparent electrode, alignment film, and a parallel-aligned nematic liquid crystal layer on top of an aluminum mirror and a silicon substrate [1]. An active matrix circuit is formed on the silicon substrate for applying voltages to pixel electrodes. Thus, the amount of phase modulation varies according to the applied voltage level. The SLM can achieve phase modulation of more than 2π radians over the visible wavelength range, and it has a phase resolution specified of 28 mrad/level. The voltage applied to each pixel in the device is assigned through a lookup table programmed in the control software. Eight-bit gray images are displayed according to the voltages applied. The pixels have a 20 μm size, and they are arranged in a 792×600 pixel display. The SLM head was connected by means of two cables to the controller unit. This unit processed the images sent from the PC

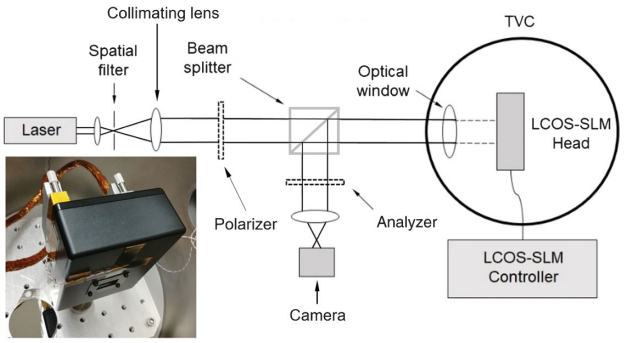


Fig. 3. Set up configuration employed to obtain the phase modulation characteristic. Picture at the bottom left side shows a view of the SLM head inside the TVC.

via the DVI-D cable and sent the suitable control signals to the SLM. Pattern generation and instrument control was performed via MATLAB.

A He–Ne laser beam was expanded and collimated to cover the whole SLM effective area ($16 \times 12\ \mathrm{mm}^2$) at normal incidence. We used an LCOS-SLM (Model X10468-01) from Hamamatsu. We used the smallest grating period achievable by the SLM (40 μm, a two pixel period). This propagated the first-order diffracted beam at 0.9° with respect to the normal. The camera (Imaging Source DMK41BU02.H) was placed where the first diffraction order overlaps the SLM reference and modulated segments, at about 0.5 m from the SLM. In our setup, the fringes had a nine-pixel camera period, large enough for fringe sampling. A beam splitter folded the SLM reflected light path so that a camera with suitable exposure time was illuminated. However, *the use of a beam splitter is not required in general*: in this setup, we used it for compactness due to the limited clear aperture of the vacuum chamber optical window.

This configuration is compatible with instrumentation that has an integrated SLM and cannot be modified. For instance, an SLM placed at the pupil of an optical system can be used with our arrangement. Assuming an imaging system such as a telescope, the laser can be used as an illumination source at the object plane of the instrument. Then, the reference grating in the SLM would be modified to contain a quadratic phase in order to guarantee a finite size of the calibration beam at the focal plane of the instrument, where, presumably, the camera of the instrument would be used to acquire the interferograms generated by our calibration procedure.

To simulate the space environment a thermal vacuum chamber (TVC) was used. The TVC has a cylinder shape with 26 cm of inner diameter and 28 cm height. It provides feedthroughs for connections to thermo-electric elements and the SLM head. In order to prevent any overheating, two thermocouples were attached to the front and back parts of the modulator. The TVC has an optical window that allows the SLM illumination, and a dedicated feedthrough was built to interface the SLM head with the controller. Finally, a primary pump and a turbo-molecular pump (Varian, Turbo-V 81-M) set the vacuum levels (10^{-5} mbar).

3. EXPERIMENTAL RESULTS

Figure 4 illustrates the phase modulation characteristic obtained with the SLM in vacuum conditions. Processing of the interferograms from the modulated segment only, and after unwrapping δ_m, results in the phase shifts illustrated in Fig. 4(a). This plot presents direct uncompensated measurements, and phase shifts present a significant scatter. In terms of qualification of optical devices for use in space applications, it is critical to understand whether this behavior is due to the SLM working in vacuum conditions, or due to the effect of the vibrations induced by the pump that affect the measurements even with the robustness intrinsic to the near-common-path setup.

However, subtraction of the environmental reference produced the plot shown in Fig. 4(b). First, it is possible to conclude that the vacuum environment is not negatively affecting the performance of the SLM, as Fig. 4(a) suggests. Second, the quality of the results reveal a nonlinear behavior in the SLM response. Indeed, data show that the root mean square error (RMSE) of a fourth-order polynomial fit was 0.334 before compensation, and 0.039 after compensation. Residuals at the bottom of each plot show clearly the uncertainty improvement.

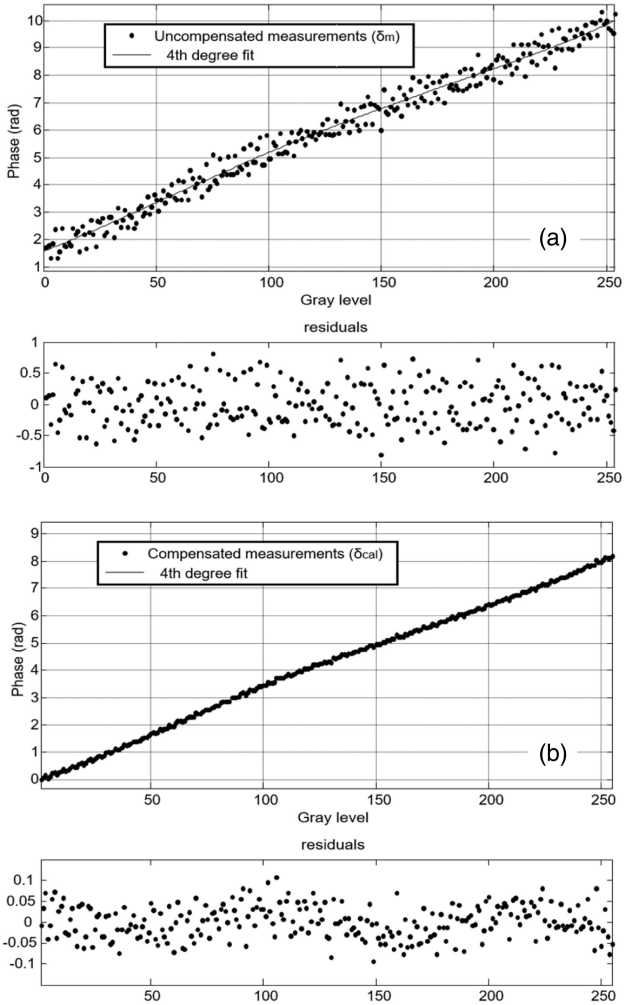


Fig. 4. SLM characteristic at vacuum conditions from (a) the modulated segment, showing a linear fit to these data with a phase resolution of 32 ± 1 mrad/level; and (b) subtraction of the modulated and reference measurements. Polynomial fit residuals are plotted below.

Table 1. RMSE of a Fourth Degree Polynomial Fit to the SLM Phase Modulation Characteristic[a]

Test Conditions	RMSE (uncomp.)	RMSE (comp.)
Room (pre-vac.)	0.055	0.027
Vacuum	0.334	0.039
Room (post-vac.)	0.051	0.049

[a]Results are listed at different test conditions. Compensated measurements show results after vibration compensation.

Table 1 shows a summary of the test campaign results. The RMSEs evaluated at different environmental conditions are listed. At vacuum conditions, we were able to confirm successful performance of the SLM due to the improved rejection of the pump vibrations. At room conditions, the improvement is not significant since there is no vibration source (vacuum pump) activated.

The results show that no sign of SLM degradation was observed. This is relevant since no special modification was performed in this commercial device before assessing its performance in vacuum conditions.

4. CONCLUSION

We presented a method to perform phase modulation characterization of an SLM under vibration conditions. The method is based on the AIA, making use of a little used output to determine the phase shifts from different segments of an SLM. The method is general and may be applied to SLMs integrated in complex optical instruments subjected to harsh environmental conditions where others methods are not applicable. This is particularly useful for end-to-end optical system tests, either on-ground or in flight conditions. It is particularly useful when using vacuum chambers since vibrations produced by the pumps easily corrupt the phase shifting measurements, making a thorough assessment of the performance of the SLM difficult. We found no sign of degradation in a commercial SLM that was subject to a vacuum test campaign. This technique can be used to calibrate SLMs integrated in optical instrumentation, where traditional interferometric arrangements are not always possible. These results also show promise in the use of SLM devices with their unique capabilities in future aerospace applications.

Funding. National Institutes of Health (K25EB024595); Ministerio de Ciencia, Innovación y Universidades (ESP2016-77548-C5-4-R, RTI2018-096886-B-C52).

Acknowledgment. The authors gratefully acknowledge Hugo Laguna and the rest of the INTA team for their technical support.

Disclosures. The authors declare no conflicts of interest.

REFERENCES

1. H. Toyoda, T. Inoue, and T. Hara, "Application of liquid crystal on silicon spatial light modulator (LCOS-SLM) for manipulation and sensing," in *14th Workshop on Information Optics (WIO)*, Kyoto, Japan, June 1, 2015, paper WS-1.
2. S. Xue, S. Chen, G. Tie, and Y. Tian, "Adaptive null interferometric test using spatial light modulator for free-form surfaces," Opt. Express **27**, 8414–8428 (2019).
3. S. Serati and J. Harriman, "Spatial light modulator considerations for beam control in optical manipulation applications," Proc. SPIE **6326**, 63262W (2006).
4. J. H. Bechtel, W. Lin, Y. Shi, and A. Yacoubian, "Electro-optic polymer integrated optic devices for space applications," Proc. SPIE **4134**, 46–55 (2000).
5. M. Silva-López, A. Campos-Jara, and A. Álvarez Herrero, "Validation of a spatial light modulator for space applications," Proc. SPIE **11180**, 111806R (2019).
6. E. W. Roberts, "Space tribology: its role in spacecraft mechanisms," J. Phys. D **45**, 503001 (2012).
7. A. Alonso, M. Reyes, and Z. Sodnik, "Performance of satellite-to-ground communications link between ARTEMIS and the optical ground station," Proc. SPIE **5572**, 372–383 (2004).
8. M. Ziemkiewicz, S. R. Davis, S. D. Rommel, D. Gann, B. Luey, J. D. Gamble, and M. Anderson, "Laser-based satellite communication systems stabilized by non-mechanical electro-optic scanners," Proc. SPIE **9828**, 982808 (2016).
9. M. Padgett, J. Courtial, and L. Allen, "Light's orbital angular momentum," Phys. Today **57**(5), 35–40 (2004).
10. Y. Takiguchi, T. Otsu, T. Inoue, and H. Toyoda, "Self-distortion compensation of spatial light modulator under temperature-varying conditions," Opt. Express **22**, 16087–16098 (2014).
11. O. Mendoza-Yero, G. Mínguez-Vega, L. Martínez-León, M. Carbonell-Leal, M. Fernández-Alonso, C. Donate-Buendía, J. Pérez-Vizcaíno, and J. Lancis, "Diffraction-based phase calibration of spatial light modulators with binary phase fresnel lenses," J. Display Technol. **12**, 14159–14171 (2016).
12. A. Lizana, N. Martin, M. Estapé, E. Fernández, I. Moreno, A. Márquez, C. Iemmi, J. Campos, and M. J. Yzuel, "Influence of the incident angle in the performance of liquid crystal on silicon displays," Opt. Express **17**, 8491–8505 (2009).
13. X. Xun and R. W. Cohn, "Phase calibration of spatially nonuniform spatial light modulator," Appl. Opt. **43**, 3910–3913 (2004).
14. D. Malacara, *Optical Shop Testing*, 2nd ed. (Wiley, 1992).
15. J. L. Martínez-Fuentes, E. J. Fernández, P. M. Prieto, and P. Artal, "Interferometric method for phase calibration in liquid crystal spatial light modulators using a self-generated diffraction-grating," Opt. Express **24**, 14159–14171 (2016).
16. P. de Groot, "Vibration in phase shifting interferometry," J. Opt. Soc. Am. A **12**, 354–365 (1995).
17. L. L. Deck, "Model-based phase shifting interferometry," Appl. Opt. **53**, 4628–4636 (2014).
18. D. M. Sycora and M. L. Holmes, "Dynamic measurements using a Fizeau interferometer," Proc. SPIE **8082**, 80821R (2011).
19. Z. Wang and B. Han, "Advanced iterative algorithm for phase extraction of randomly phase-shifted interferograms," Opt. Lett. **29**, 1671–1673 (2004).
20. J. Vargas, J. A. Quiroga, A. Ávarez Herrero, and T. Belenguer, "Phase-shifting interferometry based on induced vibrations," Opt. Express **19**, 584–596 (2011).
21. M. Silva-López, L. Bastide, R. Restrepo, P. G. Parejo, and A. Álvarez Herrero, "Evaluation of a liquid crystal based polarization modulator for a space mission thermal environment," Sens. Actuators A: Phys. **266**, 247–257 (2017).
22. S. Reichelt, "Spatially resolved phase-response calibration of liquid-crystal-based spatial light modulators," Appl. Opt. **52**, 2610–2618 (2013).
23. D. Engstron, M. Persson, J. Bengtsson, and M. Goksor, "Calibration of spatial light modulators suffering from spatially varying phase response," Opt. Express **21**, 16086–16103 (2013).